Lab on a Chip

PAPER

View Article Online
View Journal | View Issue

Cite this: *Lab Chip*, 2019, **19**, 3472

Osmotic-engine-driven liposomes in microfluidic channels†

Kan Shoji *[ab] and Ryuji Kawano *[a]

Self-propelled underwater microrobots that locomote without external sources of energy have potential application as drug carriers and probes in narrow spaces. In this study, we focused on an osmotic engine model, which is a migration mechanism, and applied it as a negative chemotaxis mechanism to induce liposome displacement. First, we confirmed the osmotic flow across the lipid bilayer and calculated the osmotic flow velocity to be 8.5 fL min^{-1} μm^{-2} when a salt concentration difference was applied to the lipid bilayer. Next, we designed and fabricated a microchannel that can trap a giant liposome and apply a salt concentration difference to the front and rear of the liposome. Then, we demonstrated the movement of the liposome by flowing it to the microchannel. The liposome successfully moved in the direction of the lower ion concentration at a speed of 0.6 μm min^{-1} owing to the osmotic pressure difference. Finally, we visualized the inner flow in the liposome by encapsulating microbeads in the liposome and observed the movement of the microbeads to verify that an osmotic flow was generated on the liposome. As a result, we observed the circulation of the microbeads in the liposome when the concentration difference was applied to the front and rear of the liposome, suggesting that the movement of the liposome was driven by the osmotic flow generated by the osmotic pressure difference. These results indicate that the osmotic-pressure-based migration mechanism has the potential to be utilized as the actuator of molecular robots.

Received 9th August 2019,
Accepted 2nd September 2019

DOI: 10.1039/c9lc00788a

rsc.li/loc

Introduction

Bio-integrated robots combining biological objects and mechanical components, such as bioactuators[1–3] and cyborg insects,[4–8] have the exclusive abilities of chemical energy driving, self-renewal capability, biocompatibility, and softness, and they can potentially be used as intracorporeal microrobots and environmental monitoring robots. Since conventional robotic systems have not yet provided these abilities, bio-integrated robots have attracted attention as novel robots. However, differences between biological objects and machines, such as materials, communication methods, and energy sources, prevent the development of fully integrated biorobots. To overcome this issue, interfaces connecting biological and mechanical objects should be designed and developed. For example, we previously reported a biofuel cell that generates electric power from insect hemolymph for the energy source of a mounted radio sensor.[7,8]

On the other hand, the concept of molecular robots whose components are artificially designed from the molecular level and assembled by bottom-up approaches has recently been proposed,[9,10] where a molecular robot is defined as a microorganism-imitating microrobot. To realize such robots, three essential components are required: sensors,[11–15] intelligence,[16] and actuators,[17–20] and they can be integrated into a unitary compartment[21–26] formed by a giant liposome, gel, and a DNA-based capsule. This cell-imitating microrobots would offer potential not only as a microrobot driving inside a body for drug delivery and diagnosis but also a biomimetic model of living cells. Molecular robots which can sense chemical signals and migrate to the chemical source by chemotaxis would show cell-like behaviors. In this way, molecular robots constructed by synthetic biology should also attract attention as a biomimetic application. Regarding the development of actuators, there are two different approaches. One is the use of molecular motors. Molecular motors, such as kinesin and myosin, are capsuled in a giant liposome and deform the liposomal membrane. For example, filopodium-like protrusions were exhibited by a giant liposome encapsulating microtubes and kinesins.[27] Furthermore, a controllable and programmable actuator that responses to a specific DNA signal has been developed by linking single-strand DNAs to a lipid membrane as an anchor of molecular motors.[19] Although these cell-imitating and molecular-motor-

[a] *Department of Biotechnology and Life Science, Tokyo University of Agriculture and Technology, 2-24-16 Naka-cho, Koganei-shi, Tokyo 184-8588, Japan. E-mail: kan-shoji@m2.tuat.ac.jp, shojikn@ucmail.uc.edu, rjkawano@cc.tuat.ac.jp*
[b] *Department of Chemistry, University of Cincinnati, Cincinnati, Ohio 45221, USA*

† Electronic supplementary information (ESI) available: Liposome formation method, hydrodynamic simulation, and bead tracking data. See DOI: 10.1039/c9lc00788a

driven actuation mechanisms have potential as biomimetic aspects of cell migration systems in synthetic biology, it is still challenging to completely imitate their structures and functions.

Another actuation mechanism is a self-propelled mechanism that induces the migration of droplets by converting external energy to mechanical motion.[28–30] These self-propelled robots are driven by either an asymmetrical chemical reaction at the leading and ending edges of the robot or the Marangoni effect caused by a surface tension gradient. These driving mechanisms are straightforward and provide stable movement compared with that for the above molecular motor systems. However, few self-propelled mechanisms using an osmotic pressure gap have been reported because a closed space must be prepared to maintain a static chemical gradient for a long time.[31]

In this study, we focus on the osmotic engine model[32] reported by Stroka and coworkers as the cell migration model. In this model, a polarized cell in which a spatial gradient of ion channels and pumps in the cell membrane is established creates a net inflow and outflow of water and ions at the cell leading and trailing edges, respectively. The net flows create net cell displacement even when the polymerization of actin in the cell is inhibited. By applying this model to a liposome, we demonstrate the emergence of chemotaxis for liposomes and propose its potential as a biomimetic model of cell migration by chemotaxis. Specifically, the semipermeability of the lipid bilayer provides net flows of water passing through the lipid bilayers owing to osmotic pressure differences at the membranes caused by the salt concentration differences between the inner and outer solutions. Although the salt concentration differences at the membranes induce osmotic flows, the salt concentration differences should be generated on the front and rear of liposomes to demonstrate the chemotaxis (the constant displacement of liposomes). Therefore, we utilize microfluidic techniques of cell trapping and gradient generation to trap liposomes and generate a salt concentration difference at the front and rear of liposomes (Fig. 1). We propose that the osmotic-pressure-based propulsion mechanism can potentially be applied to the engine of molecular robots by demonstrating liposome displacement induced by an osmotic pressure difference. Furthermore, this osmotic-pressure-driven liposome would be also useful as a simple cell migration model by chemotaxis.

Experimental

Reagents and chemicals

1,2-Dioleoyl-*sn-glycero*-3-phosphocholine (DOPC; Avanti Polar Lipid), 1,2-dioleoyl-*sn-glycero*-3-phospho-L-serine (sodium salt) (DOPS; Avanti Polar Lipid), 1,2-dioleoyl-*sn-glycero*-3-phosphoethanolamine-*N*-(lissamine rhodamine B sulfonyl) (ammonium salt) (Rhod PE; Avanti Polar Lipid), cholesterol (chol; Avanti Polar Lipid) and liquid paraffin (Wako Pure Chemical Industries, Ltd.) were used for liposome formation. DOPC and *n*-decane (Sigma-Aldrich) were used for the preparation of lipid bilayers for the observation of lipid bilayer deformation. Potassium chloride (KCl; Nacalai Tesque) and 3-morpholinopropane-1-sulfonic acid (MOPS; Nacalai Tesque) were used as aqueous solutions. The MOPS solution was prepared using ultrapure water from a Milli-Q system (Merck Millipore Corp.). Calcein (Tokyo Chemical Industry Co. Ltd.) was utilized as a dye for the fluorescence observation of liposomes. Fluoresbrite plain microspheres (diameter; 1.0 μm, Polysciences, Inc.) were used to observe the inner flow of liposomes. SU-8 3025 (MicroChem Corp.) was used as a photoresist. Polydimethylsiloxane (PDMS; Sylgard 184, Dow Corning Toray Co., Ltd.) was used for the microchannel material.

Observation of membrane deformation due to osmotic pressure difference

First, we observed the membrane deformation induced by the osmotic pressure difference acting on lipid bilayers. We prepared lipid bilayers by a droplet contact method (DCM)[33–35] and observed them under a microscope. In this method, a lipid bilayer is formed at the interface between two droplets in contact with a lipid/oil mixture. We prepared a chamber with the shape of an infinity symbol, in which two circular wells with an inner diameter of 2 mm overlapped. Lipid bilayers were prepared by inserting 2.7 μL of aqueous solution into each well, which had previously been filled with 4 μL of DOPC/*n*-decane (10 mg mL^{-1}) or DOPC : chol = 7 : 3

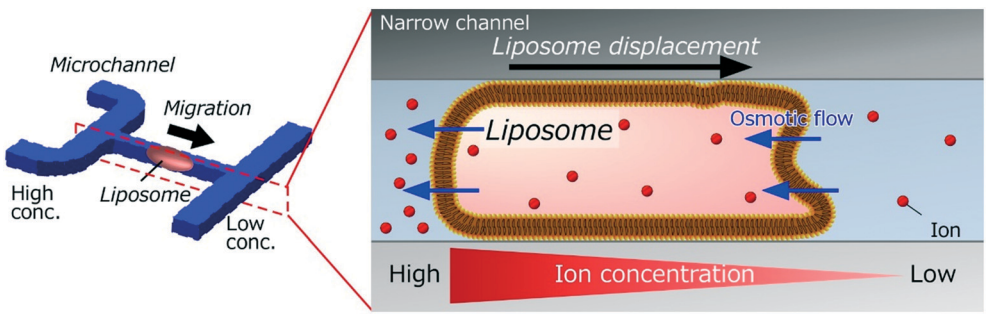

Fig. 1 Liposome-based osmotic-pressure-driven microrobot. The liposome trapped in the microchannel migrates in the direction of the lower salt concentration owing to the osmotic flow generated by the osmotic pressure difference.

(molar ratio)/*n*-decane solution. We observed and compared the membrane deformation with and without an ion concentration difference at each droplet. The observation was performed using an inverted microscope (AXJ-5300TPHFL, WRAYMER Inc.) mounted with a microscope digital camera (FLOYD, WRAYMER Inc.). The water volumes passing through the lipid bilayer were calculated by measuring the volume of droplets by image analysis (ImageJ).

Design and fabrication of the microchannel for liposome trapping and gradient generation

To generate an ion concentration difference at the front and rear of the liposome, we designed a microchannel satisfying the following requirements. First, the liposome should be tightly fixed in the microchannel to clear the gap between the liposome and the channel walls. Second, solutions with different ion concentrations must flow on both sides of the trapped liposome. Therefore, we proposed a microchannel in which strategies of a droplet-trapping microchannel[36,37] for single cell trapping and a concentration gradient microchannel[38] are combined.

To confirm the functions of the microchannel of liposome trapping and gradient generation, hydrodynamic simulations of the flow velocity and salt concentration were conducted with COMSOL Multiphysics 4.2a (COMSOL Inc.) using the microfluidics module. The density and viscosity of the aqueous solution were set to 1.0 mg mL^{-1} and 1.0 mPa s, respectively. The diffusion coefficient was set to 1.0 $\times 10^{-9}$ m^2 s^{-1}.

The microchannel was fabricated by standard photolithography techniques with SU-8 3025 which was used as the vmaster photoresist. Chromium masks were fabricated with a maskless exposure system (Nano System Solutions Inc.) as the photomasks. A mask aligner (SUSS MA6/BA6 SPEC TU, SUSS MicroTec AG) was used for UV exposure. The microchannel consists of three different layers. The first and second layers were fabricated on a single silicon wafer, and the third layer was fabricated on another silicon wafer. The channels were fabricated by PDMS molding, where PDMS was cured for 2 h at 95 °C. Each channel layer was bonded using plasma etching equipment (FA-1, Samco Inc.).

Liposome preparation and trapping in the microchannel with a salt gradient

Giant liposomes were prepared by a water-in-oil emulsion centrifugation method.[39,40] 1.0 M KCl and 0.5 mg mL^{-1} calcein solution (10 mM MOPS, pH 7.0) were contained in the liposomes. See the ESI† for further details of the formation of the giant liposomes. 1.0 M KCl solution (10 mM MOPS, pH 7.0) with liposomes and 0.1 M KCl (10 mM MOPS, pH 7.0) without liposomes flowed at 2.0 and 1.0 μL h^{-1} from inlets 1 and 2, respectively, with syringe pumps (YSP-202, YMS Co., Ltd.). We observed a liposome trapped in the narrow channel every 30 s using a fluorescence microscope (AXJ-5300TPHFL, WRAYMER Inc.) with a mounted microscope digital camera (FLOYD, WRAYMER Inc.). Then, the movements of the liposome membrane and the center of mass were measured by image analysis (ImageJ).

Observation of the inner flow with liposomes including beads

To observe the osmotic flow generated in liposomes, we prepared liposomes with fluorescent beads inside them and observed the behavior of the beads. Polystyrene fluorescent beads with a 1 μm diameter (Polysciences, Inc.) were included in the liposomes at a density of 10 beads per pL. We conducted the microfluidic experiments under the same conditions as in the above section and tracked the bead behavior.

Results and discussion

Concept and displacement mechanism of liposomes

The displacement of liposomes is based on the osmotic flow across the lipid bilayer. The semipermeability of the bilayer (water can permeate the lipid bilayer, but ions cannot) causes the osmotic flow *via* the osmotic pressure difference between inside and outside of the liposome. The osmotic pressure difference, $\Delta\Pi$, is expressed as $\Delta\Pi = \Pi_{in} - \Pi_{out} = RT(c_{in} - c_{out})$, where c_{in} and c_{out} are the ion concentrations inside and outside of the liposome, respectively. When solutions with different ion concentrations are separated by a single lipid bilayer, the water flows from the lower to the higher ion concentration owing to the osmotic pressure difference. As a result of the volume change of the solutions, the lipid bilayer moves toward the side with the lower ion concentration (Fig. 2a). Next, the case that solutions with different ion concentrations are separated by the liposome with the inner solution having an ion concentration between them is shown in Fig. 2b. Osmotic pressure is generated at the front and rear membranes of the liposome, and water flows from the lower to the higher ion concentration owing to the osmotic pressure difference at both ends of the liposome. Both membranes move in the direction of the lower ion concentration as a result of the volume change of the solutions. Finally, the liposome is transported by the shear force generated by the flexure of the membrane and migrates in the direction of the lower ion concentration.

Estimation of osmotic pressure by observing deformation of the lipid bilayer membrane

To predict the velocity of moving liposomes, the water flux passing through lipid bilayers was calculated from the deformation of the planar bilayer lipid membrane (pBLM) formed by the DCM (Fig. 3a). Because of the symmetric salt condition of 0.5 M : 0.5 M KCl in each droplet, the pBLM did not bend since it was formed with droplets of an isotonic salt solution and the osmotic pressures from both sides were equal (Fig. 3b). By contrast, the pBLM formed with droplets having

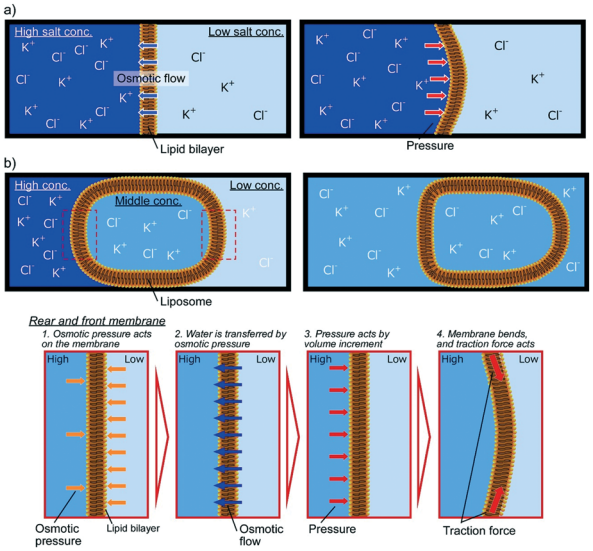

Fig. 2 Mechanism of the liposome movement. a) The case that the lipid bilayer is formed in a closed chamber. An osmotic flow passing through the pBLM from the lower to the higher salt concentration is generated when a difference in the salt concentration is generated across the lipid bilayer. Then, the lipid bilayer moves in the direction of the lower salt concentration as a result of the increased volume of the solution with the higher salt concentration. b) The case that the liposome is trapped in a closed chamber and a phased salt concentration difference is generated between the front, the inside, and the rear of the liposome. The front and rear membranes move in the direction of the lower salt concentration owing to the osmotic pressure difference, as in the case with a single lipid bilayer. Then, traction force is generated at the membrane as a result of membrane bending. Finally, the liposome migrates in the direction of the lower salt concentration.

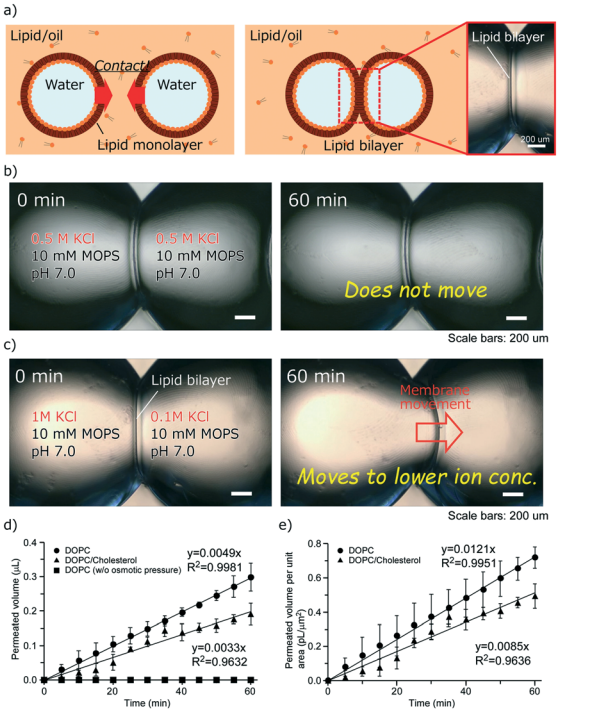

Fig. 3 a) pBLMs prepared by the DCM. pBLMs are formed by contacting lipid monolayers formed around the W/O emulsions. Microscopy images of membrane deformation b) without and c) with a salt concentration difference at each droplet. In the case of a salt concentration difference, the pBLM moves in the direction of the lower salt concentration. In contrast, the pBLM formed with isotonic droplets remains at the initial position. d) Time courses of the permeated water volume calculated by image analysis. The permeated volumes can be linearly fitted, and the flow rate is 4.9 and 3.3 nL min^{-1} with DOPC and DOPC/chol membranes. e) Time courses of the permeated water volume per unit area, which can also be linearly fitted, and the flow rate per unit area is 12.1 and 8.5 fL μm^{-2} min^{-1}, respectively.

the asymmetric salt condition of 1.0 M : 0.1 M KCl moved in the direction with the lower salt concentration because the water flowed from the lower to the higher salt concentration owing to the osmotic pressure difference at the pBLM (Fig. 3c, Movie S1†). We also observed the osmotic flow when the pBLM was formed by the lipid composition of DOPC and chol to imitate the liposomal membrane used in the liposome experiments. Although we obtained the membrane deformation with the DOPC/chol membrane, the magnitude of the deformation is smaller than that of the DOPC membrane (Fig. S1†). That is because the stiffness of the liposomal membrane increased[41] and the osmotic water permeability across the lipid bilayers decreased[42] by adding chol to the lipid membrane. From these results, we calculated the time dependence of the volume of permeated water passing through the pBLM from the volume change of the droplets (Fig. 3d). The permeated water volumes with the asymmetric salt condition of 1.0 M : 0.1 M KCl linearly increased with time in the DOPC and DOPC/chol membranes, and the flow rate of water passing through the pBLMs was calculated to be 4.9 and 3.3 nL min^{-1}, respectively.

Next, we estimated the maximum chemotaxis speed of liposomes by calculating the volume of permeated water per unit area passing through the pBLM. We assumed a rectangular shape for the pBLMs formed by the DCM.[29] The height of the pBLM was calculated to be 600 μm by the volumes of the chamber and the aqueous solution added to the chamber. The width of the pBLM was confirmed from the microscopy image and measured by ImageJ in each experiment. As a result, we confirmed that the permeated water volume per unit area also linearly increased with time, and the flow rate per unit areas with the DOPC and DOPC/chol membranes were calculated to be 12.1 and 8 fL μm^{-2} min^{-1}, respectively (Fig. 3e). Assuming that a liposome is trapped in a microfluidic channel with a 10 × 10 μm^2 cross-sectional surface, and a concentration difference with concentrations of 1.0 and 0.1 M KCl on the inside and outside of the liposome, respectively, the maximum displacement speeds of the liposomes exhibited by the DOPC and DOPC/chol membranes were estimated to be 12.1 and 8.5 μm min^{-1}, respectively. These results indicate that osmotic-flow-driven molecular robots can potentially migrate faster than molecular-motor-driven living cells, which have a migration speed of around 1 μm min^{-1} even in a microchannel.[43]

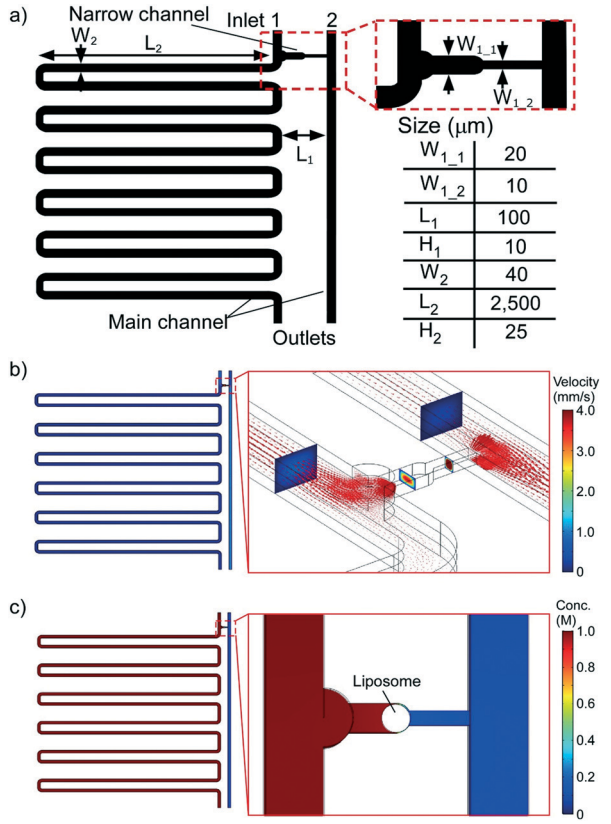

Fig. 4 a) Design of the microchannel used for liposome trapping and gradient generation. The microchannel consists of two main channels with a narrow channel connecting them. Results of the hydrodynamic simulation of b) flow velocity and c) salt concentration. Liposomes flowing in channel 1 enter the narrow channel because the resistance of the narrow channel is lower than that of channel 1. After the liposome is trapped in the narrow channel, a concentration difference is generated between the front and rear of the liposome.

Hydrodynamic simulations of the microchannel for liposome trapping and generation of concentration difference

Details of the design and the designed values of the microchannel are shown in Fig. 4a. The microchannel is composed of long and short main channels with a narrow channel connecting the two main channels. The narrow channel is divided into two parts, one is a liposome-trapping part and the other is a liposome migration part. The widths of the liposome-trapping (W_{1_1}) and the liposome migration parts (W_{1_2}) are designed to be 20 and 10 μm, respectively. The length and height of the narrow channel are 100 and 10 μm, respectively. The width and height of both main channels are designed to be 40 and 25 μm, and one of the main channels is 30 mm longer than the other so that the liposomes can flow into the narrow channel by the difference in the channel resistances between the long main channel and the narrow channel.

To trap the liposome in the microchannel and generate a concentration difference between the front and rear of the liposome, solutions with higher and lower salt concentrations and with and without liposomes were made to flow from inlets 1 and 2, respectively. The liposome from inlet 1 flows into the narrow channel because of the difference in the channel resistances between the main channel and the narrow channel. Then, the liposome is trapped in the narrow channel because its cross-sectional area (10×10 μm^2) is much smaller than the size of the liposomes (20 μm diameter). To confirm the functions of the microchannel of liposome trapping and the generation of a concentration difference between the front and rear of the trapped liposome, we calculated the flow velocity and salt concentration in the microchannel by hydrodynamic simulation.

The simulation results for the flow velocity in the microchannel are shown in Fig. 4b. In the simulation to obtain the flow velocity, the solutions flowed from inlets 1 and 2 at flow rates of 2.0 and 1.0 μL s^{-1}, respectively. The color indicates the flow velocity and the red arrows show the direction and magnitude of the flow. The solution injected from inlet 1 mainly flowed to the narrow channel, indicating that the liposome should also flow to the narrow channel. The liposome should also be trapped in the middle of the narrow channel since its diameter is expected to be around 20 μm. The simulation results of the salt concentration in the liposome-trapped and -untrapped microchannels are respectively shown in Fig. 4c and S2.† The salt concentrations of solutions injected from inlets 1 and 2 were 1.0 and 0.1 M, respectively. When the liposome is not trapped in the narrow channel, a linear concentration gradient is generated in the narrow channel. By contrast, the salt concentrations at the front and rear of the trapped liposome are almost the same as those of the injected solutions because the narrow channel is divided by the liposome. These results indicate that the microchannel can trap the liposome in the narrow channel and that a concentration difference can be generated between the front and rear of the trapped liposome.

Liposome displacement induced by the osmotic pressure difference

The microscopy image of the fabricated microchannel is shown in Fig. 5a. A solution of 1.0 M KCl (10 mM MOPS, pH 7.0) with liposomes and a solution of 0.1 M KCl (10 mM MOPS, pH 7.0) without liposomes were flowed to channels 1 and 2, respectively. The liposome flowing in channel 1 entered the narrow channel owing to the difference in the channel resistance between the narrow channel and channel 1. Then, the liposome which has a sufficiently larger size than the migration channel (10×10 μm^2) was trapped in the narrow channel (Fig. 5b, Movie S2†). Specifically, liposomes with a diameter of 15 μm or more were trapped, whereas the others passed through the narrow channel to channel 2 or were briefly trapped in the narrow channel before flowing to channel 2. After the liposomes were trapped in the narrow channel, about 50% of them ruptured or untrapped in the first 30 s. Although we first prepared liposomes formed by DOPC and attempted to trap them in the microchannel, the liposomes ruptured when they were trapped in the narrow

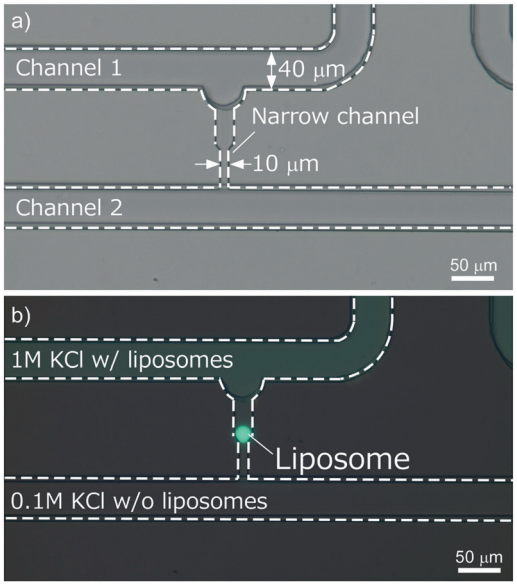

Fig. 5 a) Microscopy image of the microchannel. The widths of the narrow and main channels are 40 and 10 μm, respectively. b) Fluorescence image of the microchannel with a liposome trapped in the narrow channel. The liposome flows from channel 1 to the narrow channel and clogs the narrow channel.

channel. Hence, we formed liposomes composed of DOPC, chol, and DOPS to improve their mechanical properties (Fig. S3†).[41] Furthermore, there was no significant difference between the success rate of liposome trapping with and without the osmotic pressure, indicating that osmotic pressure did not influence the rupture of liposomes (Fig. S3†). Also, we did not observe specific membrane transformations when we applied osmotic pressure differences at the front and rear of liposomes although lipid vesicles formed with PC and cholesterol transform their shape from sphere to prolate, tube, pear, discocyte, and starfish shapes by applying a constant osmotic pressure difference.[44] We indicated that is because the osmotic pressure differences were not applied on the whole liposomes but limited membranes of liposomes (front and rear). From these results, we concluded that the stress by the flow pressure induced the rupture of liposomes due to the softness of liposomes. To improve the capture rate of liposomes, in the future, we will trap the liposomes in the microchannel with other manipulation methods such as optical tweezers.

The expansion of the front membrane of the liposome was clearly observed when 1.0 M and 0.1 M KCl were flowed in channels 1 and 2, respectively. (Fig. 6a, Movie S3†). On the other hand, the liposome did not move and remained at the

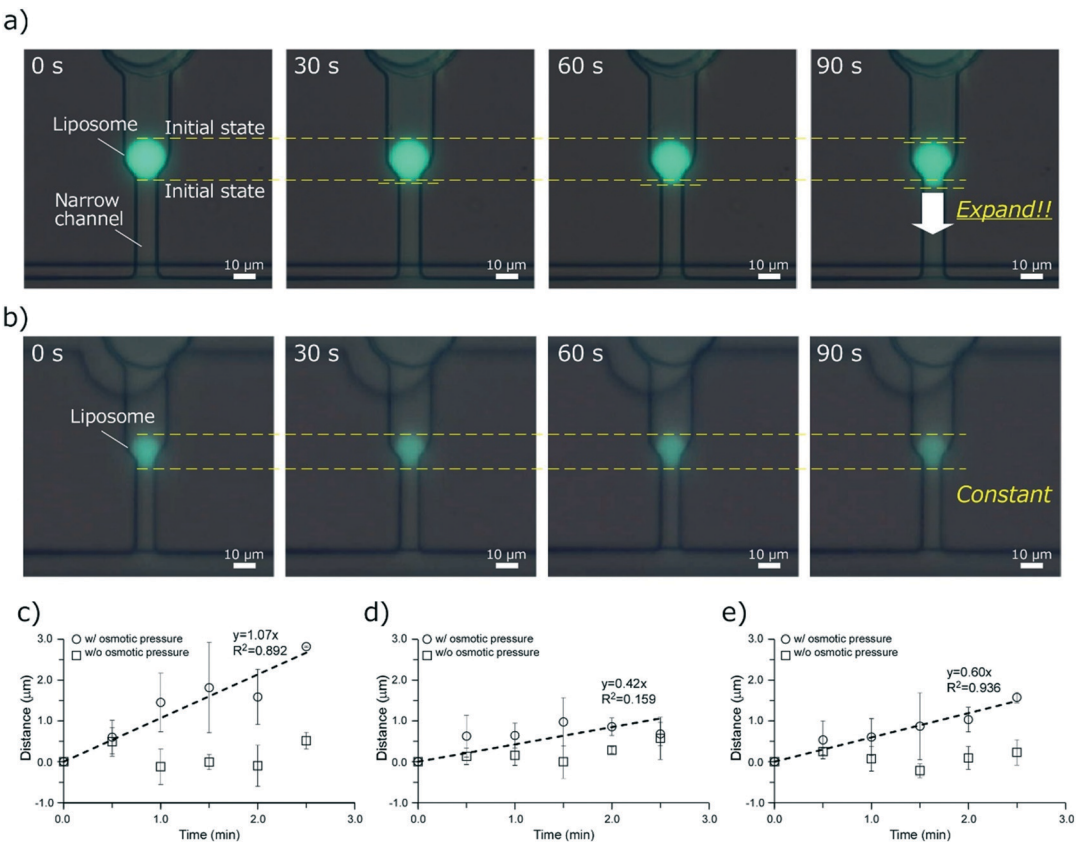

Fig. 6 Fluorescence images of a trapped liposome a) with and b) without salt concentration difference. With the salt concentration difference, the liposome moved in the direction of the lower salt concentration. Time course of the displacements of the c) front membrane, d) rear membrane, and e) center of mass of the liposome. The displacements of the front membrane and the center of mass linearly increase with time, and their speeds are 1.07 and 0.60 μm min^{-1}, respectively.

initial position under the isotonic salt conditions (Fig. 6b). The measured membrane displacements at the front and the rear of a liposome are shown in Fig. 6c and d, respectively. The front membrane of the liposome linearly expanded with a constant rate of 1.0 μm min^{-1} when the osmotic pressure difference was applied to the liposomal membrane. Although the rear membrane of the liposomes also moved in the direction of the lower salt concentration, the rate of shrinkage was lower than the rate of expansion of the front membrane. We also evaluated the displacement of the center of mass of the liposomes (Fig. 6e). The center of mass also linearly moved in the direction of the lower salt concentration with a speed of 0.60 μm min^{-1}. Because the initial salt concentrations of the front, rear, and inside of the liposome were 0.1, 1.0, and 1.0 M KCl, respectively, an osmotic flow was not initially induced at the rear membrane of the liposome. Thus, the osmotic flows at the front and rear of the liposome should have decreased and increased with decreasing salt concentration inside the liposome, respectively. Assuming that the volume of the liposome and the flow rate of the osmotic flow were 4.2 pL and 0.85 pL min^{-1}, respectively, the time required to exchange the solution inside the liposome was calculated to be about 4.9 min. Therefore, the velocity of the front membrane was greater than that of the rear membrane in the first 2.5 min. When the front membrane of the liposome has expanded by about 3 μm (about 2.5 min after the liposome was trapped in the channel), the liposome slipped and slid back. We consider that the low adhesive force between the liposomal membrane and the surface of the microchannel caused the slip. Although cells generally attach to a substrate by extracellular matrices, liposomes do not have this function and therefore slid back as a result of the traction force acting on the lipid bilayer. To drive liposomes for a long time, the adhesive force between the liposomal membrane and the substrate should be increased by electrostatic interaction or by using antibody-modified liposomes.

We visualized the internal flow of the liposomes by encapsulating fluorescent microbeads in them, and we confirmed that they were driven by the osmotic pressure difference since the liposomes had the potential to move owing to the pulsations generated by the syringe pumps. Although the microbeads did not move for a few seconds after the liposome was initially trapped in the narrow channel, several seconds after the liposome was trapped, they started to move and continued to circulate inside the liposome while the liposome was trapped in the narrow channel (Fig. 7 and Movie S4†). We indicated that this circulating flow was generated as below. First, an inflow into the liposome was induced at the front membrane of the liposome by the osmotic pressure difference. This inflow induced the one direction internal flow in the liposome. Although the outflow was generated at the rear membrane of the liposome, the flow rate was slower than that of the inflow in the first several minutes because the osmotic pressure difference at the rear membrane of the liposome was smaller than that of the front membrane. As a result, the difference between the inflow and outflow induced the circulating flow in the liposome. Also, the circulation of the microbeads expanded in the direction of the migration channel, indicating the expansion of the trapped liposome. On the other hand, the microbeads did not move and remained at their initial positions in the case of no osmotic pressure difference when the liposome was trapped in the narrow channel (Fig. S4†) or before trapping, indicating that there is no residual flow in liposomes. In addition, since there is no significant difference between the fluorescence decay rates in the trapped liposomes with and without the osmotic pressure difference, there are no holes and leakage from liposomes that might induce some flows. From these results of the microbead observation, we conclude that the osmotic flow is generated at the liposomal membrane by the osmotic pressure difference, and the liposome is moved by the osmotic engine mechanism.

Next, we compared the estimated and observed speeds of the liposome. Although the liposome formed by the DOPC and chol membrane has the potential to move at 8.5 μm min^{-1}, its actual speed was about eight times lower than the estimated value. We consider that the actual speed was mainly influenced by the friction force between the liposome membrane and the channel walls. Although the estimated speed was calculated by the water permeability passing through the lipid bilayer prepared by the DCM, there is no friction force between the chamber walls and the droplets because there is an oil layer between the droplets and the chamber walls. By contrast, the liposomes completely

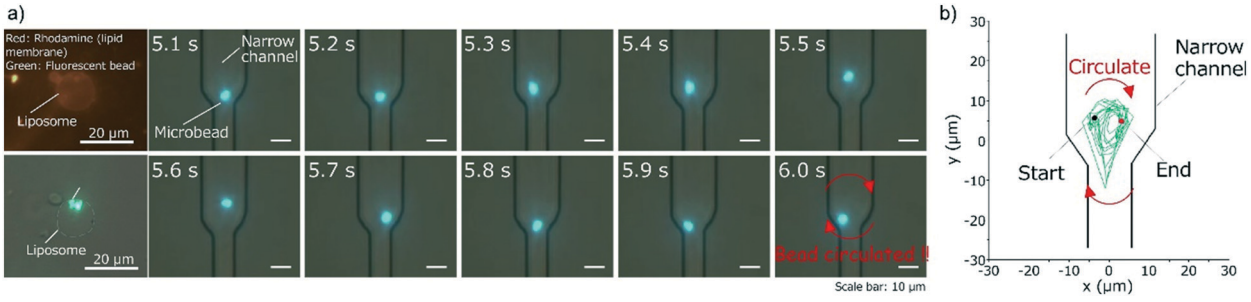

Fig. 7 a) Fluorescence images of a microbead in a liposome trapped in the narrow channel. b) Result of a tracking microbead in a liposome when a salt concentration difference is applied. The microbead circulates in the liposome, indicating an osmotic flow is generated in the liposome by the osmotic pressure difference.

attached to the channel walls, and the friction force was generated to the membrane. As a result, the expanding speed of the liposomal membrane became slower than the estimated value.

Although the velocities of conventional self-propelled robots driven by the Marangoni effect or chemical engines are faster than our osmotic-pressure-driven liposome in the order of 1–100 μm s^{-1},[45,46] our osmotic-pressure-driven liposome can move by simply applying a salt concentration difference between its front and rear without any chemical reactions. Furthermore, our method can be easily applied to liposome-based molecular robots owing to the semipermeability of their compartments. Also, the speed of our osmotic-pressure-driven liposome is almost the same as that of living cells, which is around 1 μm min^{-1},[43] suggesting that our driving mechanism has the potential to develop cell-like molecular robots.

To improve the speed of liposomes, in the future, we need to optimize the channel dimensions, the size of liposomes and the adhesion force between liposomes and channel walls. The speed of liposomes would be influenced by the channel dimensions because the traction force applied to the membrane relates to the distance of the liposomal membrane expansion and the cross-sectional dimensions of the migration channel. In this experiment, however, optimizing the channel dimensions are very difficult because we cannot completely control the size of liposomes prepared by the water-in-oil emulsion centrifugation method, which were from 5 to 30 μm in diameter (Fig. S5†). To improve the size control of liposomes, we will prepare liposomes with microfluidic techniques which can produce much uniformly sized giant liposomes.[47,48] In addition, when the trapped liposome was deformed, the elastic energy of the liposomal membrane, which tended to pull the liposome back to its initial position, increased. To overcome the energy barrier, the adhesive force between liposomes and channel walls should be controlled by surface modification on the channel walls, by electrostatic interaction, or using antibody-modified liposomes.

Conclusions

We proposed the application of an osmotic engine model to the actuator of liposome-based molecular robots. To demonstrate osmotic-pressure-driven-liposomes, we utilized the microfluidic technologies of particle trapping and gradient generation to generate a salt concentration difference between the front and rear of liposomes. As a result, we successfully induced the displacement of liposomes by the osmotic pressure difference.

To increase the speed, working time, and displacement of the liposome, we will increase the osmotic flow of water passing through the liposomal membrane by the reconstitution of an aquaporin into the liposomal membrane and control the interaction between the liposome and the channel walls by surface modification in the channel or electrostatic interaction.

For the further development of liposome-based molecular robots, the combination of osmotic-pressure and molecular-motor-driven mechanisms will enable the realization of molecular robots with advanced behavior. For example, a molecular robot that can deform its shape using molecular motors to fit a pathway and chemotactically migrate along the pathway will be developed. In addition, the reconstitution of membrane proteins and their functionalization[13,14] will also lead to the control of the osmotic-pressure-based actuation mechanism. We believe that the osmotic-pressure-driven actuation mechanism will become a breakthrough in the development of liposome-based molecular robots. Moreover, our liposome-based chemotaxis system has potential as the cell migration model to imitate the chemotaxis mechanism.

Conflicts of interest

There are no conflicts to declare.

Acknowledgements

This material is based upon work supported by the Promotion of Science (JSPS) Research Fellow and KAKENHI (Grant No. 17K19138 and 19H00901) and is partially supported by KAKENHI (Grant No. 19K15418) from the MEXT Japan.

References

1 J. Xi, J. J. Schmidt and C. D. Montemagno, *Nat. Mater.*, 2005, **4**, 180–184.
2 Y. Tanaka, K. Morishima, T. Shimizu, A. Kikuchi, M. Yamato, T. Okano and T. Kitamori, *Lab Chip*, 2006, **6**, 230–235.
3 A. W. Feinberg, A. Feigel, S. S. Shevkoplyas, S. Sheehy, G. M. Whitesides and K. K. Parker, *Science*, 2007, **317**, 1366–1370.
4 R. Holzer and I. Shimoyama, *Proceedings of the 1997 IEEE/RSJ International Conference on Intelligent Robot and Systems. Innovative Robotics for Real-World Applications. IROS '97*, 1997, vol. 3, pp. 1514–1519.
5 A. Bozkurt, J. R. F. Gilmour and A. Lal, *IEEE Trans. Biomed. Eng.*, 2009, **56**, 2304–2307.
6 H. Sato, C. W. Berry, Y. Peeri, E. Baghoomian, B. E. Casey, G. Lavella, J. M. VandenBrooks and M. M. Maharbiz, *Front. Integr. Neurosci.*, 2009, **3**, 24.
7 K. Shoji, Y. Akiyama, M. Suzuki, N. Nakamura, H. Ohno and K. Morishima, *Biosens. Bioelectron.*, 2016, **78**, 390–395.
8 K. Shoji, Y. Akiyama, N. Nakamura, H. Ohno and K. Morishima, *Proceedings of 2016 IEEE International Conference on Mechatronics and Automation (ICMA2016)*, 2016, pp. 629–634.
9 M. Hagiya, A. Konagaya, S. Kobayashi, H. Saito and S. Murata, *Acc. Chem. Res.*, 2014, **47**, 1681–1690.
10 S. Murata, A. Konagaya, S. Kobayashi, H. Saito and M. Hagiya, *New Gener. Comput.*, 2013, **31**, 27–45.
11 Y.-R. Kim, S. Jung, H. Ryu, Y.-E. Yoo, S. M. Kim and T.-J. Jeon, *Sensors*, 2012, **12**, 9530–9550.
12 M. Hiratani, M. Ohara and R. Kawano, *Anal. Chem.*, 2017, **89**, 2312–2317.

13 S. Mizukami, M. Kashibe, K. Matsumoto, Y. Hori and K. Kikuchi, *Chem. Sci.*, 2017, **8**, 3047–3053.
14 M. Ohara, M. Takinoue and R. Kawano, *ACS Synth. Biol.*, 2017, **6**, 1427–1432.
15 R. Kawano, *ChemPhysChem*, 2018, **19**, 359–366.
16 T. Masubuchi, M. Endo, R. Iizuka, A. Iguchi, D. H. Yoon, T. Sekiguchi, H. Qi, R. Iinuma, Y. Miyazono, S. Shoji, T. Funatsu, H. Sugiyama, Y. Harada, T. Ueda and H. Tadakuma, *Nat. Nanotechnol.*, 2018, **13**, 933–940.
17 M. Honda, K. Takiguchi, S. Ishikawa and H. Hotani, *Biophys. J.*, 1999, **287**, 293–300.
18 A. Roux, G. Cappello, J. Cartaud, J. Prost, B. Goud and P. Bassereau, *Proc. Natl. Acad. Sci. U. S. A.*, 2002, **99**, 5394–5399.
19 Y. Sato, Y. Hiratsuka, I. Kawamata, S. Murata and S. M. Nomura, *Sci. Robot.*, 2017, **2**, eaal3735.
20 S. Tanaka, K. Takiguchi and M. Hayashi, *Commun. Phys.*, 2018, **1**, 18.
21 T. Sunami, K. Hosoda, H. Suzuki, T. Matsuura and T. Yomo, *Langmuir*, 2010, **26**, 8544–8551.
22 S. A. Sarles and D. J. Leo, *Smart Mater. Struct.*, 2011, **20**, 094018.
23 K. Kurihara, M. Tamura, K. Shohda, T. Toyota, K. Suzuki and T. Sugawara, *Nat. Chem.*, 2011, **3**, 775–781.
24 Y. Elani, R. V. Law and O. Ces, *Nat. Commun.*, 2014, **5**, 5305.
25 L. Schoonen and J. C. M. van Hest, *Adv. Mater.*, 2016, **28**, 1109–1128.
26 C. Kurokawa, K. Fujiwara, M. Morita, I. Kawamata, Y. Kawagishi, A. Sakai, Y. Murayama, S. M. Nomura, S. Murata, M. Takinoue and M. Yanagisawa, *Proc. Natl. Acad. Sci. U. S. A.*, 2017, **114**, 7228–7233.
27 F. C. Keber, E. Loiseau, T. Sanchez, S. J. DeCamp, L. Giomi, M. J. Bowick, M. C. Marchetti, Z. Dogic and A. R. Bausch, *Science*, 2014, **345**, 1135–1139.
28 S. Sengupta, M. E. Ibele and A. Sen, *Angew. Chem., Int. Ed.*, 2012, **51**, 8434–8445.
29 M. Guix, C. C. Mayorga-Martinez and A. Merkoçi, *Chem. Rev.*, 2014, **114**, 6285–6322.
30 Z. Wu, X. Lin, T. Si and Q. He, *Small*, 2016, **12**, 3080–3093.
31 J. Nardi, R. Bruinsma and E. Sackmann, *Phys. Rev. Lett.*, 1999, **82**, 5168–5171.
32 K. M. Stroka, H. Jiang, S.-H. Chen, Z. Tong, D. Wirtz, S. X. Sun and K. Konstantopoulos, *Cell*, 2014, **157**, 611–623.
33 K. Funakoshi, H. Suzuki and S. Takeuchi, *Anal. Chem.*, 2006, **78**, 8169–8174.
34 H. Bayley, B. Cronin, A. Heron, M. A. Holden, W. L. Hwang, R. Syeda, J. Thompson and M. Wallace, *Mol. BioSyst.*, 2008, **4**, 1191–1208.
35 R. Kawano, Y. Tsuji, K. Sato, T. Osaki, K. Kamiya, M. Hirano, T. Ide, N. Miki and S. Takeuchi, *Sci. Rep.*, 2013, **3**, 1995.
36 W.-H. Tan and S. Takeuchi, *Proc. Natl. Acad. Sci. U. S. A.*, 2007, **104**, 1146–1151.
37 T. S. Kaminski and P. Garstecki, *Chem. Soc. Rev.*, 2017, **46**, 6210–6226.
38 J. Atencia, J. Morrow and L. E. Bocaccio, *Lab Chip*, 2009, **9**, 2707–2714.
39 S. Pautot, B. J. Frisken and D. A. Weitz, *Langmuir*, 2003, **19**, 2870–2879.
40 T. Toyota, N. Ohguri, K. Maruyama, M. Fujinami, T. Saga and I. Aoki, *Anal. Chem.*, 2012, **84**, 3952–3957.
41 X. Liang, G. Mao and K. Y. S. Ng, *J. Colloid Interface Sci.*, 2004, **278**, 53–62.
42 D. W. Deamer and J. Bramhall, *Chem. Phys. Lipids*, 1986, **40**, 167–188.
43 P. Maiuri, E. Terriac, P. Paul-Gilloteaux, T. Vignaud, K. McNally, J. Onuffer, K. Thorn, P. A. Nguyen, N. Georgoulia, D. Soong, A. Jayo, N. Beil, J. Beneke, J. C. H. Lim, C. P.-Y. Sim, Y.-S. Chu, A. Jiménez-Dalmaroni, J.-F. Joanny, J.-P. Thiery, H. Erfle, M. Parsons, T. J. Mitchison, W. A. Lim, A.-M. Lennon-Duménil, M. Piel and M. Théry, *Curr. Biol.*, 2012, **22**, R673–R675.
44 H. Hotani, *J. Mol. Biol.*, 1984, **178**, 113–120.
45 T. Toyota, N. Maru, M. M. Hanczyc, T. Ikegami and T. Sugawara, *J. Am. Chem. Soc.*, 2009, **131**, 5012–5013.
46 I. Lagzi, S. Soh, P. J. Wesson, K. P. Browne and B. A. Grzybowski, *J. Am. Chem. Soc.*, 2010, **132**, 1198–1199.
47 S. Matosevic and B. M. Paegel, *J. Am. Chem. Soc.*, 2011, **133**, 2798–2800.
48 N.-N. Deng, M. Yelleswarapu and W. T. S. Huck, *J. Am. Chem. Soc.*, 2016, **138**, 7584–7591.

